

ADVANCES IN ATMOSPHERIC SCIENCES

大气科学进展

EARLY ONLINE RELEASE

This is a preliminary PDF of the author-produced manuscript that has been peer-reviewed and accepted for publication in *Advances in Atmospheric Sciences*. Since it is being posted soon after acceptance, it has not yet been formatted, or processed by AAS Publications. This preliminary version of the manuscript may be downloaded, distributed, and cited, but please be aware that there will be visual differences and possibly some content differences between this version and the final published version.

The DOI for this manuscript is doi: [10.1007/s00376-018-7229-0](https://doi.org/10.1007/s00376-018-7229-0).

The final published version of this manuscript will replace the preliminary version.

If you would like to cite this EOR in a separate work, please use the following full citation:

Miao, J. P., T. Wang, H. J. Wang, and Y. Q. Gao, 2018: Influence of low-frequency solar forcing on the East Asian winter monsoon based on HadCM3 and observations. *Adv. Atmos. Sci.*, 35, <https://doi.org/10.1007/s00376-018-7229-0>.

Influence of Low-frequency Solar Forcing on the East Asian Winter Monsoon Based on HadCM3 and Observations

Jiapeng MIAO^{1,6}, Tao WANG^{*1,2}, Huijun WANG^{1,2,3,4}, and Yongqi GAO^{1,5}

¹*Nansen-Zhu International Research Center, Institute of Atmospheric Physics, Chinese Academy of Sciences, Beijing 100029, China*

²*Collaborative Innovation Center on Forecast and Evaluation of Meteorological Disasters, Nanjing University of Information Science and Technology, Nanjing 210044, China*

³*Key Laboratory of Meteorological Disaster, Nanjing University of Information Science and Technology, Nanjing 210044, China*

⁴*Climate Change Research Center, Chinese Academy of Sciences, Beijing 100029, China*

⁵*Nansen Environmental and Remote Sensing Center/Bjerknes Centre for Climate Research, Bergen 5006, Norway*

⁶*University of Chinese Academy of Sciences, Beijing 100049, China*

(Received 21 September 2017; revised 9 January 2018; accepted 16 January 2018)

ABSTRACT

In this study, we investigate the influence of low-frequency solar forcing on the East Asian winter monsoon (EAWM) by analyzing a four-member ensemble of 600-year simulations performed with HadCM3 (Hadley Centre Coupled Model, version 3). We find that the EAWM is strengthened when total solar irradiance (TSI) increases on the

*Corresponding author: Tao WANG

Email: wangtao@mail.iap.ac.cn

multidecadal time scale. The model results indicate that positive TSI anomalies can result in the weakening of Atlantic meridional overturning circulation, causing negative sea surface temperature (SST) anomalies in the North Atlantic. Especially for the subtropical North Atlantic, the negative SST anomalies can excite an anomalous Rossby wave train that moves from the subtropical North Atlantic to the Greenland Sea and finally to Siberia. In this process, the positive sea-ice feedback over the Greenland Sea further enhances the Rossby wave. The wave train can reach the Siberian region, and strengthen the Siberian high. As a result, low-level East Asian winter circulation is strengthened and the surface air temperature in East Asia decreases. Overall, when solar forcing is stronger on the multidecadal time scale, the EAWM is typically stronger than normal. Finally, a similar linkage can be observed between the EAWM and solar forcing during the period 1850--1970.

Key words: solar forcing, East Asian winter monsoon, Atlantic sea surface temperature, Rossby wave train

1. Introduction

Previous studies have illustrated the influences of solar variability on the climate of Earth (e.g., Haigh, 2001; Lean and Rind, 2001; Rind, 2002; Meehl et al., 2003; Meehl et al., 2008; Xiao et al., 2017). In the stratosphere, for example, solar-induced ozone changes can affect the temperature and zonal wind distribution, the mechanisms for which have been described in Gray et al. (2010) and many references therein. Correspondingly, the Northern Hemisphere polar vortex responds obviously to the 11-year solar cycle, although it is also influenced by the quasi-biennial oscillation (Labitzke, 1987; Labitzke and Van Loon, 1988). In the

troposphere, the Hadley and Walker circulations strengthen during peak solar years, and the Intertropical Convergence Zone and South Pacific Convergence Zone shift poleward (van Loon et al., 2004, 2007). Furthermore, observational and modeling studies have reported the influences of solar variability on the North Atlantic Oscillation (NAO) (Shindell et al., 2001; Kodera, 2002; Swingedouw et al., 2011; Gray et al., 2013). In addition, the 11-year solar cycle can be detected at the surface of Earth. Meehl et al. (2008) and Meehl and Arblaster (2009) observed a La Niña-like cold event at the peak sunspot number (SSN) followed by an El Niño-like event a few years later. Huo and Xiao (2016) noted that solar activity might have contributed to the El Niño Modoki component of the 2015/16 El Niño event. Furthermore, some studies have indicated that the global surface temperature is significantly related to the 11-year solar cycle (Tung and Camp, 2008; Zhou and Tung, 2010; Huo and Xiao, 2017). The monsoon rainfalls in India, South Asia, West Africa, and North America also exhibit high correlations with solar variability (Kodera, 2004; van Loon et al., 2004).

The East Asian winter monsoon (EAWM), which is the most distinct climate system over East Asia in winter (Lau and Li, 1984; Tao and Chen, 1987; He et al., 2007), is influenced by both internal variability and external forcings (Ding et al., 2014). For instance, the variability in the EAWM is closely related to the major mode of atmospheric variability, such as the Arctic Oscillation and the NAO (Gong et al., 2001; Wu and Wang, 2002; Sung et al., 2010; He et al., 2017). The Pacific sea surface temperature (SST) also plays an important role in EAWM variability (Yang et al., 2002; Zhou et al., 2007a; Sun et al., 2016), especially the El Niño–Southern Oscillation (ENSO) over the tropical Pacific (Zhang et al., 1996, 1999; Wang et al., 2000; Zhou et al., 2007b; Wang and He, 2012). For example, Wang et al. (2000)

indicated that the warm (cold) phase ENSO cycle is typically related to a weak (strong) EAWM and the western North Pacific anticyclone (cyclone) acts as a bridge between phases. Additionally, the Atlantic Multidecadal Oscillation (AMO) is associated with the East Asian winter climate (Li and Bates, 2007; Wang et al., 2009). Both modeling and observational studies have reported that the warm phase of the AMO can lead to warmer than average conditions in East Asia in boreal winter. Additionally, some recent studies have shown the influences of Arctic sea-ice loss and Arctic amplification on the EAWM, although no consensus has been reached (Wang and Liu, 2016; Zhou, 2017). From the perspective of external forcing, some studies have projected weakened EAWM low-level northerlies under global warming scenarios (Hu et al., 2000; Hori and Ueda, 2006). A recent modeling study suggests that the projected low-level northerly winds could be enhanced over the Northeast Asian coastal region, Southeast Asia, and the South China Sea, but with little change over midlatitude East Asia (Xu et al., 2016). In addition, Jiang et al. (2017), based on CAM5 simulations, suggested that anthropogenic aerosols can intensify the EAWM northern mode. Furthermore, a recent study found that strong tropical volcanic eruptions play an important role in regulating the EAWM (Miao et al., 2016).

However, until recently, the influence of solar variability on the EAWM had received little attention. Those studies that have now explored this topic used reanalysis and observational data from the late 20th century and concluded that the EAWM weakens as solar activity strengthens on the interannual time scale (Weng, 2012; Wang et al., 2015). However, the response of the EAWM to solar forcing on a longer time scale remains unclear. Therefore, in this study, we investigate the effect of low-frequency solar variability on the East Asian

winter (December, January and February) climate using an ensemble of simulations involving only solar forcing variability, which excludes the influences of anthropogenic agents. Observational and reanalysis data collected before the 1970s are also used in this study. We describe the model, data and methods in section 2. In section 3, we investigate the influence of low-frequency solar forcing on the EAWM. Conclusions and discussion are given in section 4.

2. Model, data and methods

The model used in this study is the Hadley Centre Coupled Model, version 3 (HadCM3) (Gordon et al., 2000; Pope et al., 2000). The atmospheric component of HadCM3 is a version of the UKMO's Unified Model. The model is run on a $3.75^\circ \times 2.5^\circ$ longitude–latitude grid and has 19 hybrid levels in the vertical direction. This version incorporates significant improvements compared to the previous version (Pope et al., 2000). The ocean component is a version of the Cox (1984) model, with a $1.25^\circ \times 1.25^\circ$ horizontal grid. Six ocean grid squares correspond to one atmospheric model grid square. The ocean model has 20 vertical levels, and the resolution near the ocean surface is enhanced. The atmospheric and ocean models are coupled once daily, and the details can be found in Gordon et al. (2000). HadCM3 can be run without flux adjustments, and it has been widely used to simulate past and future climate change. For example, when all anthropogenic and natural forcings are included, the HadCM3-simulated surface air temperature (SAT) agrees well with instrumental data and reconstruction ensemble datasets over the past millennium (Schurer et al., 2014). More details of the model components and performance can be found in Schurer et al. (2014) and the references therein.

A four-member ensemble of HadCM3 simulations spanning from 1400 to 2000 is analyzed in this study (Schurer et al., 2013). The simulations are run with only solar forcing variability, while other forcings (such as well-mixed greenhouse gases, land use, and orbital forcing) are set to constants (1400 levels). The solar forcing used here is the reconstruction of total solar irradiance (TSI) from Steinhilber et al. (2009) between 1400 and 1810, and from Wang et al. (2005) between 1810 and 2000. The Wang et al. (2005) reconstruction datasets with and without background information are linearly combined to make the two reconstructions match. The TSI series is shown in Fig. 1. The four ensembles are initialized with the same oceanic conditions as those in 1400, but different atmospheric conditions near the 1400. These conditions are from a long-term simulation of all relevant forcings beginning in 800 AD. More details of the initialization method can be found in Schurer et al. (2014).

In addition, we use sea level pressure (SLP) from HadSLP2r [Second Hadley Centre Sea Level Pressure dataset near-real time product (Allan and Ansell, 2006)] to investigate the influences of solar forcing on the EAWM in the observations. A Siberian high index is defined as the mean SLP over the region (40° – 60° N, 70° – 120° E) (Gong et al., 2001). The SSN is used to represent the solar variability in the observational analysis (available from <http://sidc.oma.be/silso/yearlyssnplot>) and is a direct expression of the intensity of solar activity. Thus, we can avoid problems associated with using TSI, which is reconstructed under various assumptions (Gray et al., 2013).

In this study, we focus on the low-frequency climate variability associated with TSI variability. The low-pass Lanczos filtering method is applied to the TSI series and all the fields with a 13-year cutoff period. Notably, the Schwabe cycle can be filtered via this

method. The statistical significance of the regression analyses is estimated using a “random phase” test, which can eliminate the low-pass filtering-induced serial correlation effects (Ebisuzaki, 1997).

3. Results

3.1 Evaluation of modeled climatology

We first evaluate the model climatology over East Asia in winter. This evaluation verifies the credibility of the following analysis and the conclusions based on this model. Considering the general characteristics of the EAWM, we examine the climatologies of the SAT, SLP and 850-hPa winds here. As shown in Fig. 2b, the simulated SAT is distributed latitudinally and generally decreases northward. Large-scale cooling can be observed over the Tibetan Plateau. This pattern agrees well with observations (Fig. 2a). However, some biases also exist. The model overestimates the SAT to the west of Lake Baikal and underestimates the SAT over the Tibetan Plateau and in Northeast China (Fig. 3c). In winter, the Siberian high and Aleutian low are located over the Asian continent and North Pacific, respectively (Fig. 2d). The model almost fully captures the spatial patterns of the two systems, but it does not effectively reproduce the center of the Siberian high (Fig. 2e). Additionally, the model underestimates the intensity of the Siberian high (Fig. 2f). For the low-level circulation, the EAWM is characterized by the northwesterly winds over northeastern Asia and northeasterly winds over the South China Sea (Fig. 2g). Clearly, the model reproduces the wind fields well, although some discrepancies exist (Figs. 2h and i). Overall, HadCM3 can simulate the large-scale EAWM circulation effectively, and this result supports the following analysis.

3.2 Influences of solar forcing on the EAWM in the model

A strengthened Siberian high is often considered a characteristic of a strong EAWM (Guo, 1994; Gong et al., 2001). As shown in Fig. 3a, anomalously positive SLPs are evident over Siberia and East China when the TSI is high on the multidecadal time scale. These SLPs reflect an enhancement of the Siberian high. Their consistent trends can be seen from the time series of TSI and Siberian high index (Fig. 1). Both time series exhibit decreasing trends during the periods 1401–60, 1580–1700, 1780–1820 and 1860–80; whereas, they show increasing trends during the periods 1460–1560, 1700–60, 1820–60 and 1880–1999. As a result, when the TSI is high, anomalous anticyclones can be observed over the high-latitude Eurasian continent (Fig. 3b). Additionally, northerly wind anomalies are present over East Asia, indicating an anomalously strengthened low-level East Asian winter circulation. Correspondingly, more cold air can be brought southward to low-latitude regions. Thus, significant surface cooling is observed over East and North China (Fig. 3c). Overall, the EAWM typically strengthens when solar forcing strengthens in the model.

To understand the possible mechanisms of the intensified Siberian high, we first examine the response of large-scale atmospheric circulation over the Northern Hemisphere to low-frequency changes in TSI. When TSI is high, positive 500-hPa geopotential height (Z500) anomalies are present over Siberia and southern Iceland (Fig. 4a). Correspondingly, negative Z500 anomalies are evident over the Greenland Sea and subtropical North Atlantic. The alternating occurrence of negative–positive–negative–positive anomalies resembles a Rossby wave pattern that propagates from the subtropical North Atlantic to the Siberian region. We further investigate the corresponding quasi-geostrophic stream function and wave activity

flux (WAF) anomalies, which can reflect the propagation of stationary Rossby waves and indicate the direction of energy propagation (Takaya and Nakamura, 2001). As shown in Fig. 4b, the wave train propagates northeastward from the subtropical North Atlantic to the Iceland basin and then splits into two branches. One branch propagates eastward and reaches the Siberian region. This branch is weak (non-significant). The other branch continues northward to the Greenland Sea and then swings toward the Siberian region. This northward branch of the Rossby wave is significantly strengthened when it reaches the Greenland Sea, which is likely due to the positive feedback of sea ice there (Fig. 5a). When this wave train reaches the Siberian region, the convergence of the WAF can strengthen the Siberian high.

The formation of a Rossby wave is highly correlated with thermal and orographic forcing (Hoskins and Karoly, 1981). As shown in Fig. 4b, the origin of this wave train is over the subtropical North Atlantic. Thus, it is likely that this negative–positive–negative–positive wave train is excited by negative SST-induced convective heating anomalies over the subtropical North Atlantic (Fig. 5b). Significant cooling over the subtropical North Atlantic can decrease the latent heat flux and moisture flux to the atmosphere. These changes subsequently decrease convective instability. Therefore, convective heating is reduced over the subtropics, and excitation of the Rossby wave train occurs, as illustrated in Fig. 4b. The anomalous subtropical North Atlantic SST likely plays an important role in shaping this Rossby wave train and related atmospheric circulation anomalies over East Asia. To confirm this inferred linkage, we define a SST-cooling index over the subtropical North Atlantic (20° – 30° N, 40° – 70° W; black frame in Fig. 5b). The regression maps on it show a similar negative–positive–negative–positive wave train from the subtropical North Atlantic to Siberia

(Figs. 6a and b). As a result, the Siberian high is significantly strengthened, causing significant surface cooling over East Asia (Figs. 6c and d). Therefore, the negative SST anomalies over the subtropical North Atlantic are the main reason for the formation of the wave train and the strengthening of the EAWM when TSI is high. However, it should be noted that the southern (northern) branch of the wave train is relatively stronger (weaker) compared to that in the TSI-related process. This suggests that the positive feedback of sea ice over the Greenland Sea probably plays an important role in strengthening the northern Rossby wave in the TSI-related process (Fig. 5a).

Thus, the relationship between changes in TSI and negative SST anomalies over the subtropical North Atlantic should be considered. Most regions of the North Atlantic exhibit negative SST anomalies when TSI is high. In contrast, positive SST anomalies can be observed over the entire tropical and South Atlantic. This northern negative and tropical (southern) positive SST anomaly pattern reflects the weakening of the Atlantic meridional overturning circulation (AMOC). For confirmation, we illustrate the response of the AMOC stream function to solar forcing in Fig. 7. Significant negative stream function anomalies across the Atlantic cell indicate a reduction in AMOC strength. In addition, the negative sea surface salinity anomalies in the North Atlantic also indicate a weakened AMOC (Fig. 8). As noted in previous modeling studies (Latif et al., 2009; Otterå et al., 2010; Swingedouw et al., 2011), positive TSI anomalies lead to an increase in surface heat flux, which induces negative buoyancy forcing and a decrease in mixed layer depth in the Labrador Sea. Thus, the decreased convection in the Labrador Sea can weaken the AMOC. This process is similar to responses of the AMOC to global warming (Gregory et al., 2005). Therefore, the negative

SST anomalies over the subtropical North Atlantic are mainly caused by the TSI-induced weakening of the AMOC. Additionally, reduced northward heat transport due to a weakened AMOC decreases the SST in the high-latitude Atlantic (Fig. 9), which can increase the sea-ice coverage over the Greenland Sea. This process explains the strengthened wave train in the Greenland Sea area.

3.3 Observed influences of solar forcing on the EAWM

Based on observations, a similar relationship can be found between the low-frequency solar activity and Siberian high during the period 1850--1970. As shown in Fig. 10a, both the SSN and Siberian high index exhibit decreasing trends from 1850--1910 and increasing trends from 1910--1970. This means that the SSN and Siberian high index have consistent trends during 1850--1970, similar to the findings from the model results (Fig. 1). Figure 10b shows a regression map of the SLP in winter associated with solar forcing during the period 1850--1970. Positive SLP anomalies can be observed over the Siberian region. These findings suggest strong EAWM circulation. However, this relationship reverses after the 1970s. The regression map shows negative SLP anomalies over the high-latitude Eurasian continent when the SSN is high during the period 1971--2014 (Fig. 10c).

4. Summary and discussion

This study investigates the response of the EAWM to solar forcing in HadCM3. The results suggest that low-frequency TSI variability plays an important role in regulating the intensity of the EAWM, particularly the Siberian high. The model results show that positive TSI anomalies can weaken the AMOC and cause negative SST anomalies in the North

Atlantic. Especially for the subtropical North Atlantic, the negative SST anomalies can excite a Rossby wave train that moves from the subtropical North Atlantic to the Greenland Sea and finally to the Siberian region. In this process, the positive sea-ice feedback over the Greenland Sea further enhances the eastward propagation of the Rossby wave. When the wave train reaches Siberia, the Siberian high is strengthened. As a result, northerly wind anomalies are present over East Asia, indicating anomalously strengthened low-level East Asian winter circulation. In addition, surface cooling can be observed over East Asia. Therefore, the EAWM is strengthened due to the high TSI on the multidecadal time scale.

During the period 1850--1970, a similar linkage can be observed between the low-frequency solar activity and the Siberian high. The trends of the SSN and Siberian high index on the multidecadal time scale are consistent. It suggests that higher SSN can lead to a stronger East Asian monsoon circulation. However, this linkage reverses during the period 1971--2014. Why this relationship between the SSN and Siberian high reverses remains unclear. However, complex external forcings, such as rapid increases in greenhouse gas concentrations during the second half of the 20th century, may modulate this relationship. Specifically, the influence of intensive anthropogenic aerosol emissions over East Asia from the 1970s (Wang et al., 2013) on the Asian regional climate is much stronger than that associated with solar activity. These emissions can also modulate the linkage between the SSN and Siberian high. It is well known that the Siberian high controls almost the entire Asian continent in boreal winter, and the corresponding anticyclonic circulation causes northerly winds over eastern China (Gong et al., 2001). The intensity of the Siberian high plays a dominant role in determining the intensity of the EAWM (Guo, 1994). As a result, the

reversed relationship between the SSN and Siberian high after the 1970s also reflects the reversed linkage between the SSN and EAWM circulation. Explanations for this phenomenon require further investigation.

A recent modeling study gives a different explanation regarding the linkage between the solar activity and SST over the North Atlantic (Thiéblemont et al., 2015). An anomalous tripolar SST pattern in winter of the peak solar year was found and attributed to the solar maximum-induced positive NAO phase. This is a fast response and it operates on the 11-year solar cycle time frame. However, our study focuses on influences from a low-frequency (longer than 11-year cycle) solar forcing on the EAWM. According to our analysis and a previous modeling study (Swingedouw et al., 2011), there are no significant relationships between the NAO and TSI at this time scale. In our study, we attribute the SST anomalies over the North Atlantic to the TSI-induced weakening of the AMOC.

In this study, the model does not include stratospheric ozone changes from the ultraviolet part of the solar spectrum. Thus, the mechanism mainly depends on the solar forcing acting on the ocean surface (bottom-up process). Actually, the solar signals in the stratosphere can affect the EAWM through stratosphere-troposphere coupling (top-down process) (Wang et al., 2015). It should be determined whether these two mechanisms act together or play opposing roles in regulating the EAWM. A similar study of the tropical Pacific was presented by Meehl et al. (2009), who compared three climate models with mechanisms acting alone and acting together. An analysis of the EAWM using this method should be performed in the future.

Acknowledgments. This research was supported by the National Natural Science Foundation of China (Grant Nos. 41575086 and 41661144005), and the CAS–PKU (Chinese Academy of Sciences–Peking University) Joint Research Program.

REFERENCES

- Allan, R., and T. Ansell, 2006: A new globally complete monthly historical gridded mean sea level pressure dataset (HadSLP2): 1850--2004. *J. Climate*, **19**, 5816--5842, <https://doi.org/10.1175/JCLI3937.1>.
- Cox, M. D., 1984: A primitive equation, 3-dimensional model of the ocean. GFDL Ocean Group Technical Rep 1. Princeton NJ, USA, 143 pp.
- Ding, Y. H., and Coauthors, 2014: Interdecadal variability of the east asian winter monsoon and its possible links to global climate change. *Journal of Meteorological Research*, **28**, 693--713, <https://doi.org/10.1007/s13351-014-4046-y>.
- Ebisuzaki, W., 1997: A method to estimate the statistical significance of a correlation when the data are serially correlated. *J. Climate*, **10**, 2147--2153, [https://doi.org/10.1175/1520-0442\(1997\)010<2147:AMTETS>2.0.CO;2](https://doi.org/10.1175/1520-0442(1997)010<2147:AMTETS>2.0.CO;2).
- Gong, D. Y., S. W. Wang, and J. H. Zhu, 2001: East Asian winter monsoon and Arctic Oscillation. *Geophys. Res. Lett.*, **28**, 2073--2076, <https://doi.org/10.1029/2000GL012311>.
- Gordon, C., C. Cooper, C. A. Senior, H. Banks, J. M. Gregory, T. C. Johns, J. F. B. Mitchell, and R. A. Wood, 2000: The simulation of SST, sea ice extents and ocean heat transports in a version of the Hadley Centre coupled model without flux adjustments. *Climate Dyn.*, **16**, 147--168, <https://doi.org/10.1007/s003820050010>.

Gray, L. J., and Coauthors, 2010: Solar influences on climate. *Rev. Geophys.*, **48**, RG4001, <https://doi.org/10.1029/2009RG000282>.

Gray, L. J., and Coauthors, 2013: A lagged response to the 11 year solar cycle in observed winter Atlantic/European weather patterns. *J. Geophys. Res.*, **118**, 13405--13420,

<https://doi.org/10.1002/2013JD020062> Gregory, J. M., and Coauthors, 2005: A model intercomparison of changes in the Atlantic thermohaline circulation in response to increasing atmospheric CO₂ concentration. *Geophys. Res. Lett.*, **32**, L12703, <https://doi.org/10.1029/2005GL023209>

Guo, Q. Y., 1994: Relationship between the variations of East Asian winter monsoon and temperature anomalies in China. *Quarterly Journal of Applied Meteorology*, **5**, 218--225. (in Chinese)

Haigh, J. D., 2001: Climate variability and the influence of the sun. *Science*, **294**, 2109--2111, <https://doi.org/10.1126/science.1067013>.

He, J. H., J. H. Ju, Z. P. Wen, J. M. Lu, and Q. H. Jin, 2007: A review of recent advances in research on Asian monsoon in China. *Adv. Atmos. Sci.*, **24**, 972--992, <https://doi.org/10.1007/s00376-007-0972-2>.

He, S. P., Y. Q. Gao, F. Li, H. J. Wang, and Y. C. He, 2017: Impact of arctic oscillation on the East Asian climate: A review. *Earth-Science Reviews*, **164**, 48--62, <https://doi.org/10.1016/j.earscirev.2016.10.014>.

Hori, M. E., and H. Ueda, 2006: Impact of global warming on the East Asian winter monsoon as revealed by nine coupled atmosphere-ocean GCMs. *Geophys. Res. Lett.*, **33**, L03713, <https://doi.org/10.1029/2005GL024961>.

- Hoskins, B. J., and D. J. Karoly, 1981: The steady linear response of a spherical atmosphere to thermal and orographic forcing. *J. Atmos. Sci.*, **38**, 1179--1196, [https://doi.org/10.1175/1520-0469\(1981\)038<1179:TSLROA>2.0.CO;2](https://doi.org/10.1175/1520-0469(1981)038<1179:TSLROA>2.0.CO;2).
- Hu, Z. Z., L. Bengtsson, and K. Arpe, 2000: Impact of global warming on the Asian winter monsoon in a coupled GCM. *J. Geophys. Res.*, **105**, 4607--4624, <https://doi.org/10.1029/1999JD901031>.
- Huo, W.-J., and Z.-N. Xiao, 2016: The impact of solar activity on the 2015/16 El Niño event. *Atmos. Oceanic Sci. Lett.*, **9**, 428--435, <https://doi.org/10.1080/16742834.2016.1231567>.
- Huo, W.-J., and Z.-N. Xiao, 2017: Anomalous pattern of ocean heat content during different phases of the solar cycle in the tropical Pacific. *Atmos. Oceanic Sci. Lett.*, **10**, 9--16, <https://doi.org/10.1080/16742834.2017.1247412>.
- Jiang, Y. Q., and Coauthors, 2017: Anthropogenic aerosol effects on East Asian winter monsoon: The role of black carbon-induced Tibetan Plateau warming. *J. Geophys. Res.*, **122**, 5883--5902, <https://doi.org/10.1002/2016JD026237>.
- Kodera, K., 2002: Solar cycle modulation of the North Atlantic Oscillation: Implication in the spatial structure of the NAO. *Geophys. Res. Lett.*, **29**, 1218, <https://doi.org/10.1029/2001GL014557>.
- Kodera, K., 2004: Solar influence on the Indian Ocean Monsoon through dynamical processes. *Geophys. Res. Lett.*, **31**, L24209, <https://doi.org/10.1029/2004GL020928>.
- Labitzke, K., 1987: Sunspots, the QBO, and the stratospheric temperature in the north polar region. *Geophys. Res. Lett.*, **14**, 535--537, <https://doi.org/10.1029/GL014i005p00535>.

- Labitzke, K., and H. Van Loon, 1988: Associations between the 11-year solar cycle, the QBO and the atmosphere. Part I: The troposphere and stratosphere in the northern hemisphere in winter. *J. Atmos. Terr. Phys.*, **50**, 197--206, [https://doi.org/10.1016/0021-9169\(88\)90068-2](https://doi.org/10.1016/0021-9169(88)90068-2).
- Latif, M., W. Park, H. Ding, and N. S. Keenlyside, 2009: Internal and external North Atlantic sector variability in the Kiel climate model. *Meteor. Z.*, **18**, 433--443, <https://doi.org/10.1127/0941-2948/2009/0395>.
- Lau, K.-M., and M.-T. Li, 1984: The monsoon of East Asia and its global associations—a survey. *Bull. Amer. Meteor. Soc.*, **65**, 114--125, [https://doi.org/10.1175/1520-0477\(1984\)065<0114:TMOEAA>2.0.CO;2](https://doi.org/10.1175/1520-0477(1984)065<0114:TMOEAA>2.0.CO;2).
- Lean, J., and D. Rind, 2001: Earth's response to a variable sun. *Science*, **292**, 234--236, <https://doi.org/10.1126/science.1060082>.
- Li, S. L., and G. T. Bates, 2007: Influence of the Atlantic multidecadal oscillation on the winter climate of East China. *Adv. Atmos. Sci.*, **24**, 126--135, <https://doi.org/10.1007/s00376-007-0126-6>.
- Meehl, G. A., and J. M. Arblaster, 2009: A lagged warm event-like response to peaks in solar forcing in the Pacific region. *J. Climate*, **22**, 3647--3660, <https://doi.org/10.1175/2009JCLI2619.1>.
- Meehl, G. A., W. M. Washington, T. M. L. Wigley, J. M. Arblaster, and A. Dai, 2003: Solar and greenhouse gas forcing and climate response in the Twentieth century. *J. Climate*, **16**, 426--444.

- Meehl, G. A., J. M. Arblaster, G. Branstator, and H. van Loon, 2008: A coupled air-sea response mechanism to solar forcing in the Pacific region. *J. Climate*, **21**, 2883--2897, <https://doi.org/10.1175/2007JCLI1776.1>.
- Meehl, G. A., J. M. Arblaster, K. Matthes, F. Sassi, and H. van Loon, 2009: Amplifying the pacific climate system response to a small 11-year solar cycle forcing. *Science*, **325**, 1114--1118, <https://doi.org/10.1126/science.1172872>.
- Miao, J. P., T. Wang, Y. L. Zhu, J. Z. Min, H. J. Wang, and D. Guo, 2016: Response of the East Asian winter monsoon to strong tropical volcanic eruptions. *J. Climate*, **29**, 5041--5057, <https://doi.org/10.1175/JCLI-D-15-0600.1>.
- Otterå, O. H., M. Bentsen, H. Drange, and L. L. Suo, 2010: External forcing as a metronome for Atlantic multidecadal variability. *Nature Geoscience*, **3**, 688--694, <https://doi.org/10.1038/ngeo955>.
- Pope, V. D., M. L. Gallani, P. R. Rowntree, and R. A. Stratton, 2000: The impact of new physical parametrizations in the Hadley Centre climate model: HadAM3. *Climate Dyn.*, **16**, 123--146, <https://doi.org/10.1007/s003820050009>.
- Rind, D., 2002: The sun's role in climate variations. *Science*, **296**, 673--677, <https://doi.org/10.1126/science.1069562>.
- Schurer, A., S. F. B. Tett, M. Mineter, and G. C. Hegerl, 2013: Euroclim500---Causes of change in European mean and extreme climate over the past 500 years: Climate variable output from HadCM3 numerical model. NCAS British Atmospheric Data Centre.

- Schurer, A. P., S. F. B. Tett, and G. C. Hegerl, 2014: Small influence of solar variability on climate over the past millennium. *Nature Geoscience*, **7**, 104--108, <https://doi.org/10.1038/ngeo2040>.
- Shindell, D. T., G. A. Schmidt, M. E. Mann, D. Rind, and A. Waple, 2001: Solar forcing of regional climate change during the maunder minimum. *Science*, **294**, 2149--2152, <https://doi.org/10.1126/science.1064363>.
- Steinhilber, F., J. Beer, and C. Fröhlich, 2009: Total solar irradiance during the Holocene. *Geophys. Res. Lett.*, **36**, L19704, <https://doi.org/10.1029/2009GL040142>.
- Sun, J. Q., S. Wu, and J. Ao, 2016: Role of the North Pacific sea surface temperature in the East Asian winter monsoon decadal variability. *Climate Dyn.*, **46**, 3793--3805, <https://doi.org/10.1007/s00382-015-2805-9>.
- Sung, M.-K., G.-H. Lim, and J.-S. Kug, 2010: Phase asymmetric downstream development of the North Atlantic Oscillation and its impact on the East Asian winter monsoon. *J. Geophys. Res.*, **115**, D09105, <https://doi.org/10.1029/2009JD013153>.
- Swingedouw, D., L. Terray, C. Cassou, A. Voltaire, D. Salas-Méla, and J. Servonnat, 2011: Natural forcing of climate during the last millennium: Fingerprint of solar variability. *Climate Dyn.*, **36**, 1349--1364, <https://doi.org/10.1007/s00382-010-0803-5>.
- Takaya, K., and H. Nakamura, 2001: A formulation of a phase-independent wave-activity flux for stationary and migratory quasigeostrophic eddies on a zonally varying basic flow. *J. Atmos. Sci.*, **58**, 608--627, [https://doi.org/10.1175/1520-0469\(2001\)058<0608:AFOAPI>2.0.CO;2](https://doi.org/10.1175/1520-0469(2001)058<0608:AFOAPI>2.0.CO;2).

- Tao, S. Y., and L. X. Chen, 1987: A review of recent research on the East Asian summer monsoon in China. *Monsoon Meteorology*, C. P. Chang and T. N. Krishnamurti, Eds., Oxford University Press, 60--92.
- Thiéblemont, R., K. Matthes, N.-E. Omrani, K. Kodera, and F. Hansen, 2015: Solar forcing synchronizes decadal North Atlantic climate variability. *Nature Communications*, **6**, 8268, <https://doi.org/10.1038/ncomms9268>.
- Tung, K. K., and C. D. Camp, 2008: Solar cycle warming at the Earth's surface in NCEP and ERA-40 data: A linear discriminant analysis. *J. Geophys. Res.*, **113**, D05114, <https://doi.org/10.1029/2007JD009164>.
- van Loon, H., G. A. Meehl, and J. M. Arblaster, 2004: A decadal solar effect in the tropics in July–August. *Journal of Atmospheric and Solar-Terrestrial Physics*, **66**, 1767--1778, <https://doi.org/10.1016/j.jastp.2004.06.003>.
- van Loon, H., G. A. Meehl, and D. J. Shea, 2007: Coupled air-sea response to solar forcing in the Pacific region during northern winter. *J. Geophys. Res.*, **112**, D02108, <https://doi.org/10.1029/2006JD007378>.
- Wang, B., R. G. Wu, and X. H. Fu, 2000: Pacific-East Asian teleconnection: How does ENSO affect East Asian climate? *J. Climate*, **13**, 1517--1536, [https://doi.org/10.1175/1520-0442\(2000\)013<1517:PEATHD>2.0.CO;2](https://doi.org/10.1175/1520-0442(2000)013<1517:PEATHD>2.0.CO;2).
- Wang, H. J., and S. P. He, 2012: Weakening relationship between East Asian winter monsoon and ENSO after mid-1970s. *Chinese Science Bulletin*, **57**, 3535--3540, <https://doi.org/10.1007/s11434-012-5285-x>.

- Wang, R. L., Z. N. Xiao, K. Y. Zhu, and Z. T. Gao, 2015: Asymmetric impact of solar activity on the east asian winter climate and its possible mechanism. *Chinese Journal of Atmospheric Sciences*, **39**, 815--826, <https://doi.org/10.3878/j.issn.1006-9895.1410.14211>. (in Chinese)
- Wang, S.-Y., and J. P. Liu, 2016: Delving into the relationship between autumn Arctic sea ice and central–eastern Eurasian winter climate. *Atmos. Oceanic Sci. Lett.*, **9**, 366--374, <https://doi.org/10.1080/16742834.2016.1207482>.
- Wang, T., H. J. Wang, O. H. Otterå, Y. Q. Gao, L. L. Suo, T. Furevik, and L. Yu, 2013: Anthropogenic agent implicated as a prime driver of shift in precipitation in eastern China in the late 1970s. *Atmos. Chem. Phys.*, **13**, 12 433--12 450, <https://doi.org/10.5194/acp-13-12433-2013>.
- Wang, Y. M., J. L. Lean, and N. R. Sheeley, Jr., 2005: Modeling the sun's magnetic field and irradiance since 1713. *The Astrophysical Journal*, **625**, 522--538, <https://doi.org/10.1086/429689>.
- Wang, Y. M., S. L. Li, and D. H. Luo, 2009: Seasonal response of Asian monsoonal climate to the Atlantic multidecadal oscillation. *J. Geophys. Res.*, **114**, D02112, <https://doi.org/10.1029/2008JD010929>.
- Weng, H. Y., 2012: Impacts of multi-scale solar activity on climate. Part I: Atmospheric circulation patterns and climate extremes. *Adv. Atmos. Sci.*, **29**, 867--886, <https://doi.org/10.1007/s00376-012-1238-1>.
- Wu, B. Y., and J. Wang, 2002: Winter arctic oscillation, siberian high and East Asian winter monsoon. *Geophys. Res. Lett.*, **29**, 1897, <https://doi.org/10.1029/2002GL015373>.

- Xiao, Z. N., D. L. Li, L. M. Zhou, L. Zhao, and W. J. Huo, 2017: Interdisciplinary studies of solar activity and climate change. *Atmos. Oceanic Sci. Lett.*, **10**, 325--328, <https://doi.org/10.1080/16742834.2017.1321951>.
- Xu, M. M., H. M. Xu, and J. Ma, 2016: Responses of the East Asian winter monsoon to global warming in CMIP5 models. *Int. J. Climatol.*, **36**, 2139--2155, <https://doi.org/10.1002/joc.4480>.
- Yang, S., K.-M. Lau, and K.-M. Kim, 2002: Variations of the East Asian jet stream and Asian-Pacific-American winter climate anomalies. *J. Climate*, **15**, 306--325, [https://doi.org/10.1175/1520-0442\(2002\)015<0306:VOTEAJ>2.0.CO;2](https://doi.org/10.1175/1520-0442(2002)015<0306:VOTEAJ>2.0.CO;2).
- Zhang, R. H., A. Sumi, and M. Kimoto, 1996: Impact of El Niño on the East Asian monsoon: A diagnostic study of the '86/87 and '91/92 events. *J. Meteor. Soc. Japan*, **74**, 49--62, https://doi.org/10.2151/jmsj1965.74.1_49.
- Zhang, R. H., A. Sumi, and M. Kimoto, 1999: A diagnostic study of the impact of El Niño on the precipitation in China. *Adv. Atmos. Sci.*, **16**, 229--241, <https://doi.org/10.1007/BF02973084>.
- Zhou, J. S., and K.-K. Tung, 2010: Solar cycles in 150 years of global sea surface temperature data. *J. Climate*, **23**, 3234--3248, <https://doi.org/10.1175/2010JCLI3232.1>.
- Zhou, W., 2017: Impact of Arctic amplification on East Asian winter climate. *Atmos. Oceanic Sci. Lett.*, **10**, 385--388, <https://doi.org/10.1080/16742834.2017.1350093>.
- Zhou, W., C. Y. Li, and X. Wang, 2007a: Possible connection between Pacific Oceanic interdecadal pathway and east Asian winter monsoon. *Geophys. Res. Lett.*, **34**, L01701, <https://doi.org/10.1029/2006GL027809>.

Zhou, W., X. Wang, T. J. Zhou, C. Li, and J. C. L. Chan, 2007b: Interdecadal variability of the relationship between the East Asian winter monsoon and ENSO. *Meteor. Atmos. Phys.*, **98**, 283--293, <https://doi.org/10.1007/s00703-007-0263-6>.

PRELIMINARY ACCEPTED VERSION

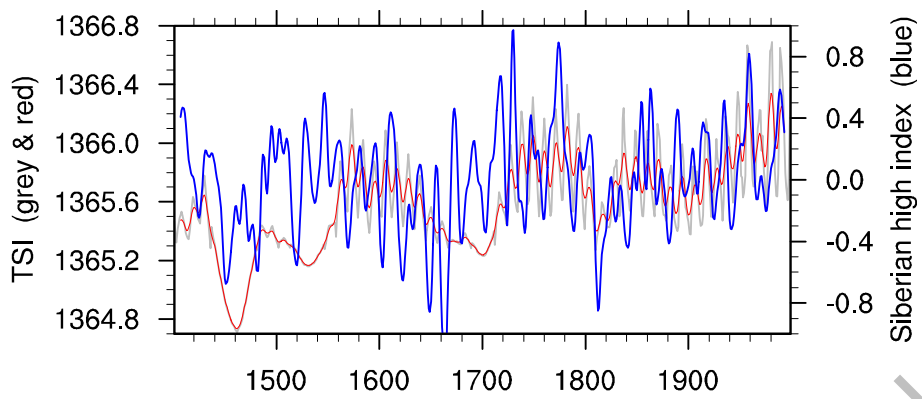


Fig. 1. Time series of TSI (units: W m^{-2}) and Siberian high index during 1401–1999. The red (blue) line represents the low-pass filtered TSI (Siberian high index) series with a 13-year cutoff period, while the gray line represents the unfiltered TSI series.

PRELIMINARY ACCEPTED VERSION

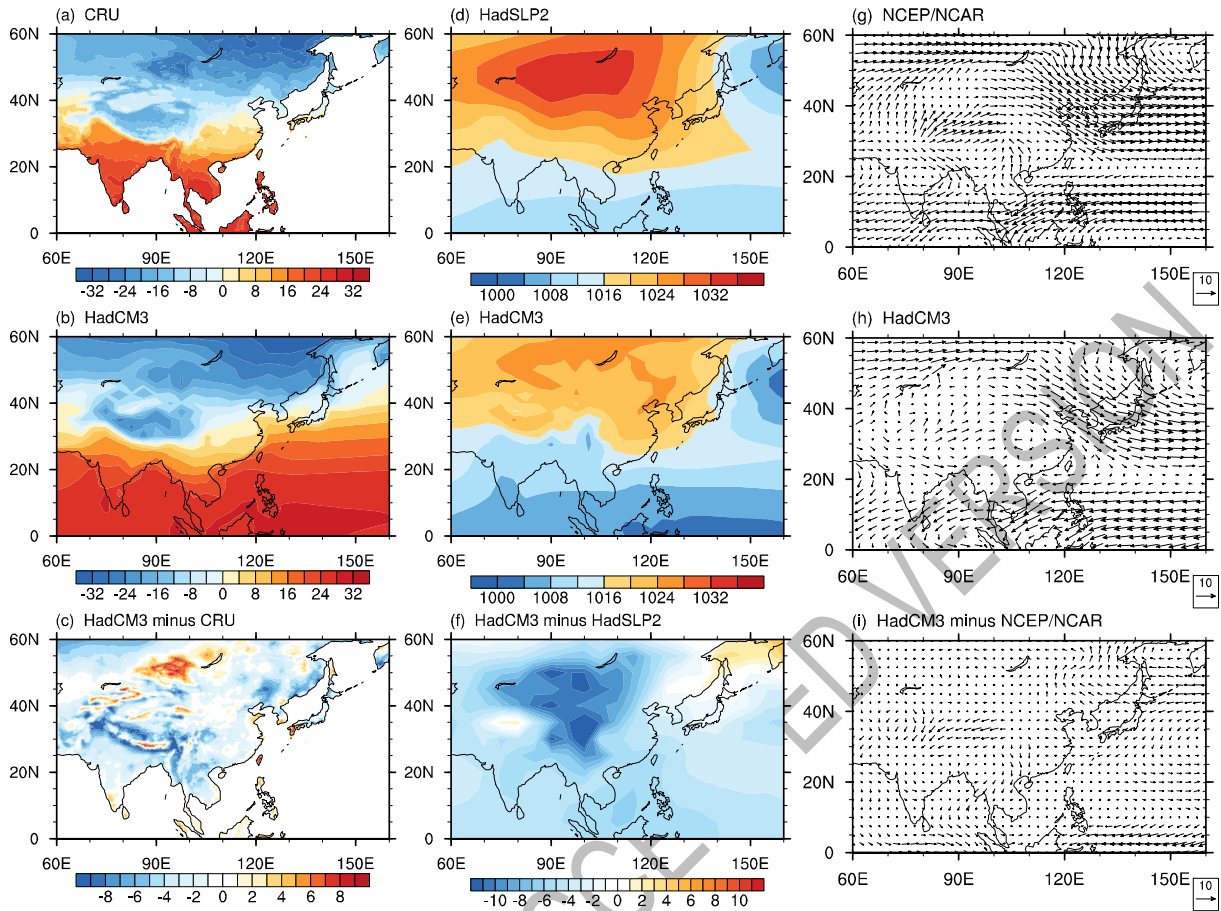


Fig. 2. Climatology of winter mean (a) SAT (1901--99; units: °C), (d) SLP (1850--1999; units: hPa) and (g) 850-hPa winds (1948--99; units: m s^{-1}) based on the observational and reanalysis data. (b, e, h) As in (a, d, g) but based on the HadCM3 model results over the period 1401--1999. (c, f, i) Differences between the model and observational data.

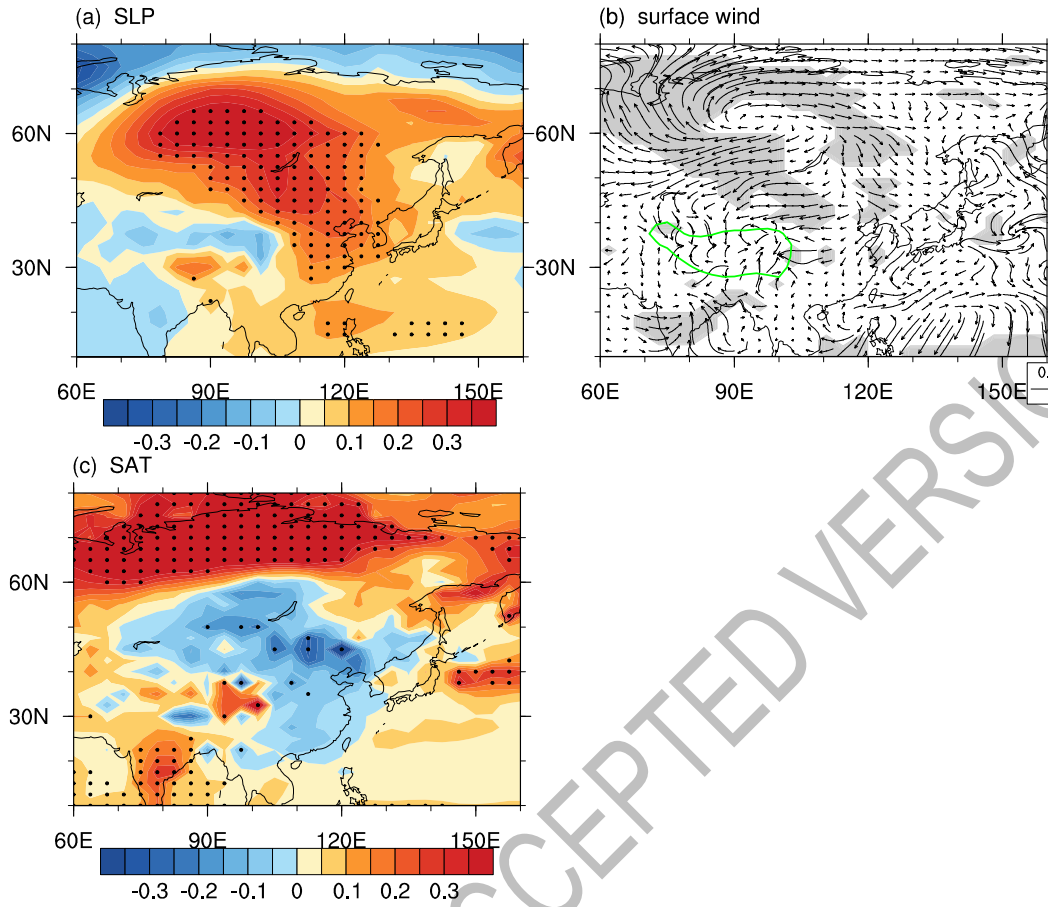


Fig. 3. Regression of the winter (a) SLP (units: hPa), (b) surface wind (units: m s^{-1}), and (c) SAT (units: $^{\circ}\text{C}$) on the TSI (units: W m^{-2}) during 1401--1999 in the simulation. The TSI and atmospheric variables have been low-pass filtered with a 13-year cutoff period. Areas significant at the 95% confidence level are marked with dots in (a, c) but shaded in gray in (b). The green line in (b) shows the 3000 m topographic contour.

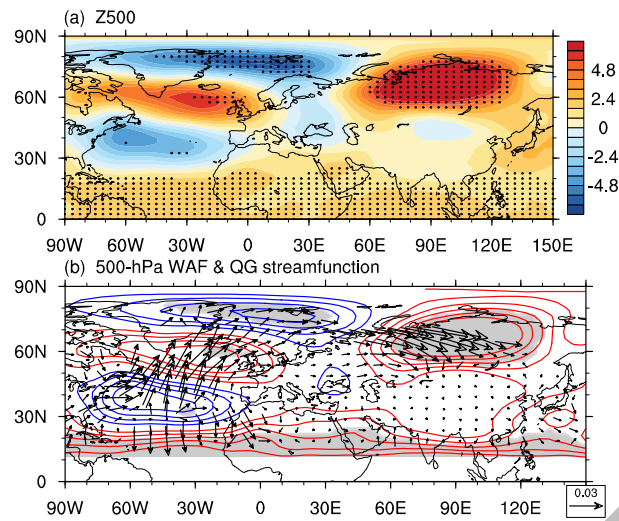


Fig. 4. Regression of the winter (a) Z500 (units: m) and (b) 500-hPa quasi-geostrophic streamfunction (contours; units: $10^5 \text{ m}^2 \text{ s}^{-1}$) and WAF (vectors; units: $\text{m}^2 \text{ s}^{-2}$) on the TSI (units: W m^{-2}) during 1401--1999 in the simulation. Blue (red) lines represent negative (positive) values, and the contour interval is 10^5 (units: $\text{m}^2 \text{ s}^{-1}$) in (b). The TSI and atmospheric variables have been low-pass filtered with a 13-year cutoff period. Areas significant at the 95% confidence level are marked with dots in (a) but shaded in (b).

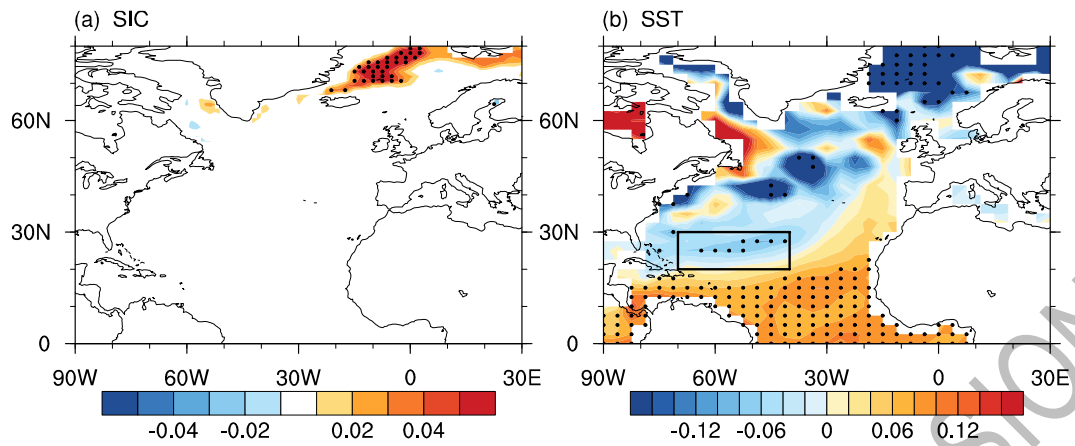


Fig. 5. Regression of the winter (a) sea-ice concentration and (b) SST (units: °C) on the TSI (units: W m^{-2}) during 1401--1999 in the simulation. The TSI and oceanic variables have been low-pass filtered with a 13-year cutoff period. Areas significant at the 95% confidence level are marked with dots. The black frame (20° – 30° N, 40° – 70° W) in (b) is used to define a SST-cooling index.

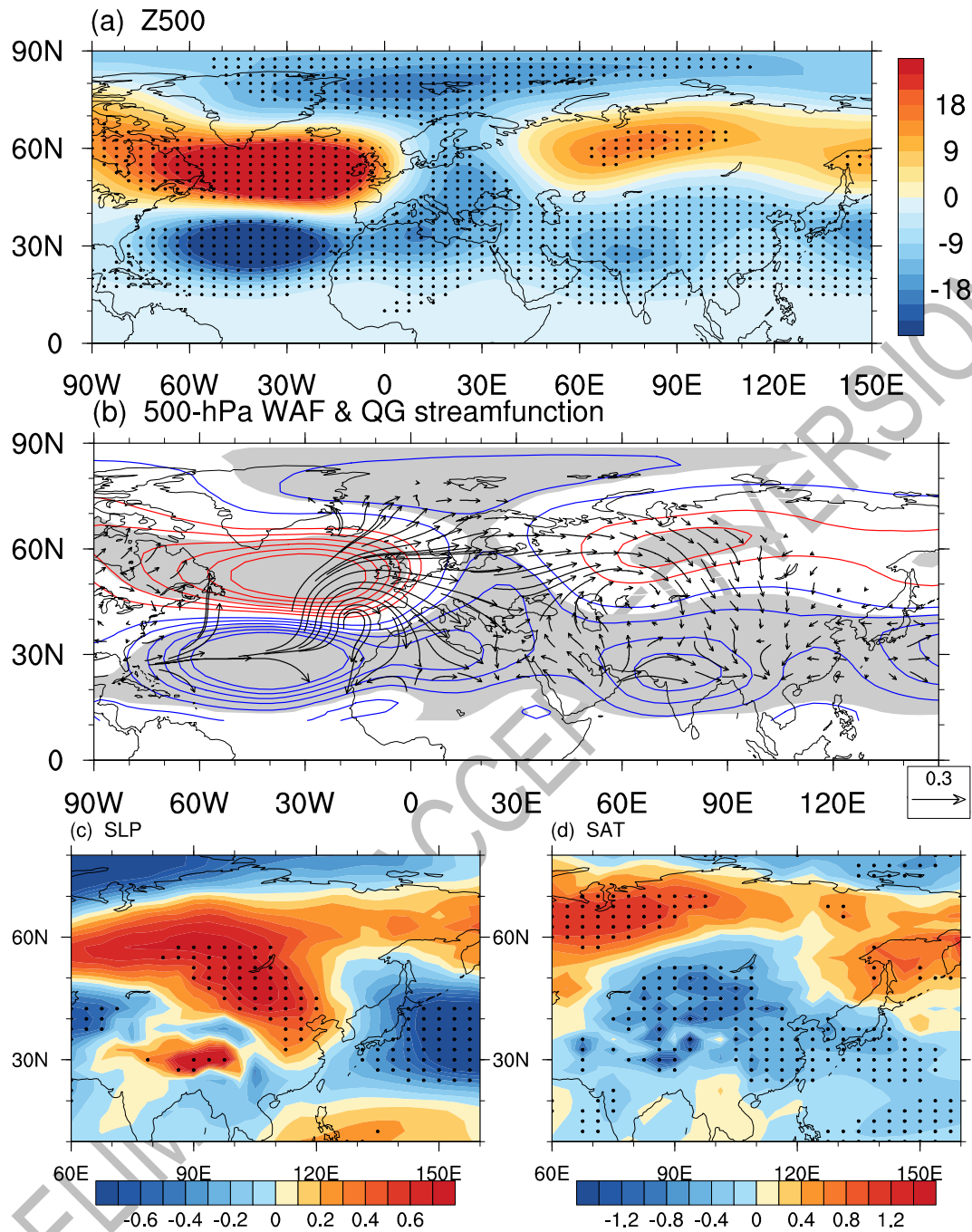


Fig. 6. Regression of the winter (a) 500-hPa geopotential height (units: m), (b) 500-hPa quasi-geostrophic stream function (contours; units: $10^5 \text{ m}^2 \text{ s}^{-1}$) and WAF (vectors; units: $\text{m}^2 \text{ s}^{-2}$), (c) SLP (units: hPa), and (d) SAT (units: $^{\circ}\text{C}$) on the SST index (units: $^{\circ}\text{C}$) during 1401--1999 in the simulation. Blue (red) lines represent negative (positive) values, and the

contour interval is 5×10^5 (units: $\text{m}^2 \text{s}^{-1}$) in (b). Areas significant at the 95% confidence level are marked with dots in (a, c, d) but shaded in gray in (b).

PRELIMINARY ACCEPTED VERSION

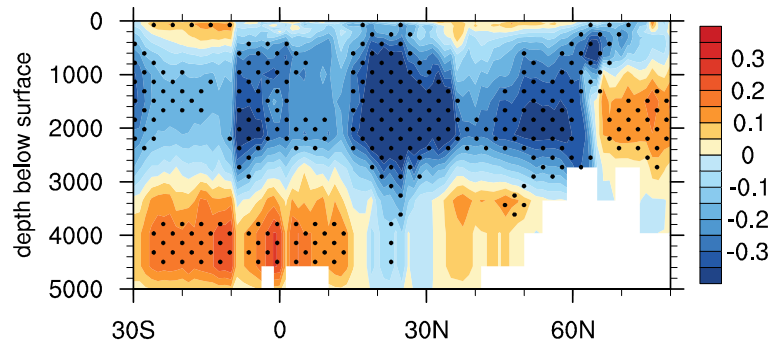


Fig. 7. Regression of the winter Atlantic meridional overturning stream function (units: Sv) on the TSI (units: W m^{-2}) during 1401--1999 in the simulation. The TSI and oceanic variables have been low-pass filtered with a 13-year cutoff period. Areas significant at the 95% confidence level are marked with dots.

PRELIMINARY ACCEPTED VERSION

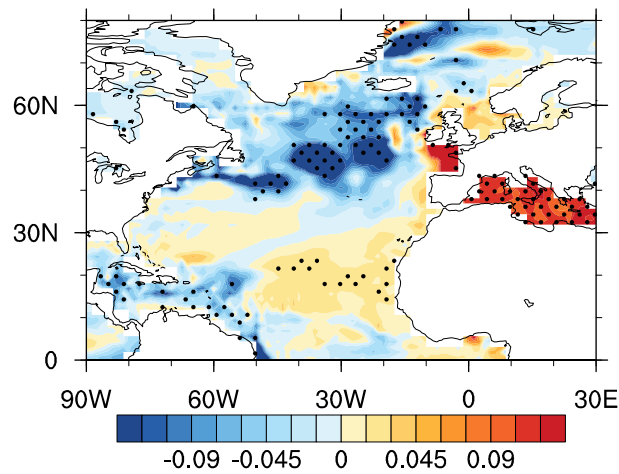


Fig. 8. Regression of the winter sea surface salinity (units: psu) and the TSI (units: W m^{-2}) during 1401--1999 in the simulation. The TSI and oceanic variables have been low-pass filtered with a 13-year cutoff period. Areas significant at the 95% confidence level are marked with dots.

PRELIMINARY ACCEPTED VERSION

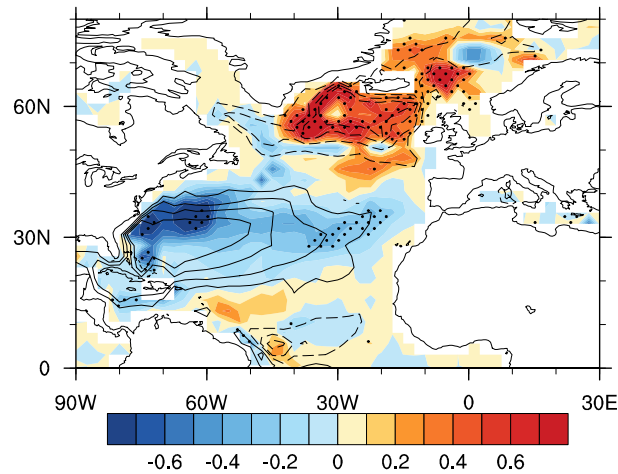


Fig. 9 Regression of the winter ocean barotropic stream function (color shading; units: Sv) and the TSI (units: W m^{-2}) during 1401--1999 in the simulation. The TSI and oceanic variables have been low-pass filtered with a 13-year cutoff period. Areas significant at the 95% confidence level are marked with dots. The contours show the climatological winter ocean barotropic stream function (interval: 5 Sv; zero-line omitted), with solid (dashed) lines meaning positive (negative).

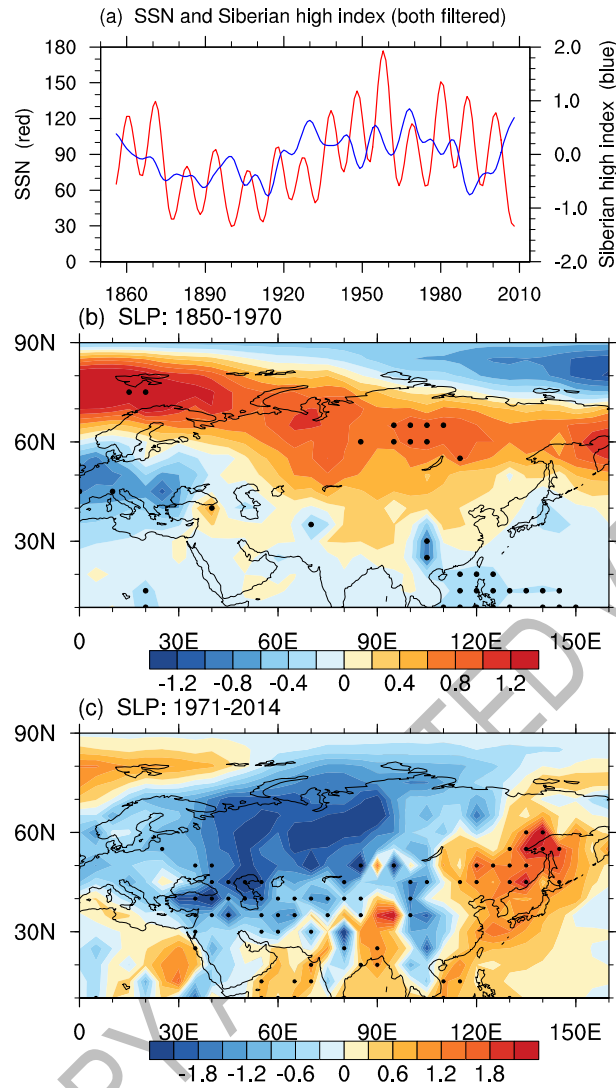


Fig. 10. (a) Time series of SSN (red) and Siberian high index (blue) during 1850–2014. (b, c) Regression of the winter SLP (units: hPa) on the SSN over the period (b) 1850–1970 and (c) 1971–2014 in the observations. The SSN and atmospheric variables have been low-pass filtered with a 13-year cutoff period. Areas significant at the 90% confidence level are marked with dots.